Is the impact sensitivity of RDX polymorph dependent?

Is the impact sensitivity of RDX polymorph dependent?

Imogen L. Christopher,[a] Colin R. Pulham,[a] Adam A. L. Michalchuk,[b,*] and Carole A. Morrison [a,*]

School of Chemistry and EaSTCHEM Research School, University of Edinburgh, David Brewster Road, The King's Buildings, Edinburgh, EH9 3FJ, UK.

School of Chemistry, University of Birmingham, Edgebaston, Birmingham, B15 2TT, UK.

Email: C.Morrison@ed.ac.uk

Abstract

Impact-sensitivity predictions based on the vibrational up-pumping model show a strong polymorph dependency for RDX and highlight that one of the high-pressure forms, which has been postulated to form during shock-wave experiments, is appreciably more susceptible to mechanical initiation. The origin of the predicted impact sensitivity variation can be attributed to vibrational mode hardening by pressure and to differences in the molecular conformation of RDX in the four polymorphs studied. These polymorphs present different distributions of molecular vibrations within their respective up-pumping windows, which leads to their varying ability to up-pump and trap the vibrational energy that arises from mechanical insult.

Introduction

The ease of initiating energetic materials (explosives, propellants, gas generators and pyrotechnics, EMs) by impact and shock are essential parameters from both an application and safety standpoint.[1] Impact sensitivity (IS) is typically measured by a drop-hammer apparatus, where a known mass is dropped from a variable height until the minimum energy threshold required to induce initiation is established. However, despite the existence of well-established testing protocols, it is not uncommon for variable results to be reported by different laboratories, with temperature, humidity, sample purity, crystallinity, particle size, and operator experience all known to affect the outcome of the binary 'go/no-go' call.[2] In many EM research labs, RDX (formally hexahydro-1,3,5-trinitro-1,3,5-triazine, see Figure 1) has been informally adopted as a laboratory internal standard for IS measurements, allowing the sensitivities of novel materials to be ranked in comparison to this widely characterised EM. However, there is substantial variability in the reported IS values of RDX itself. [2]

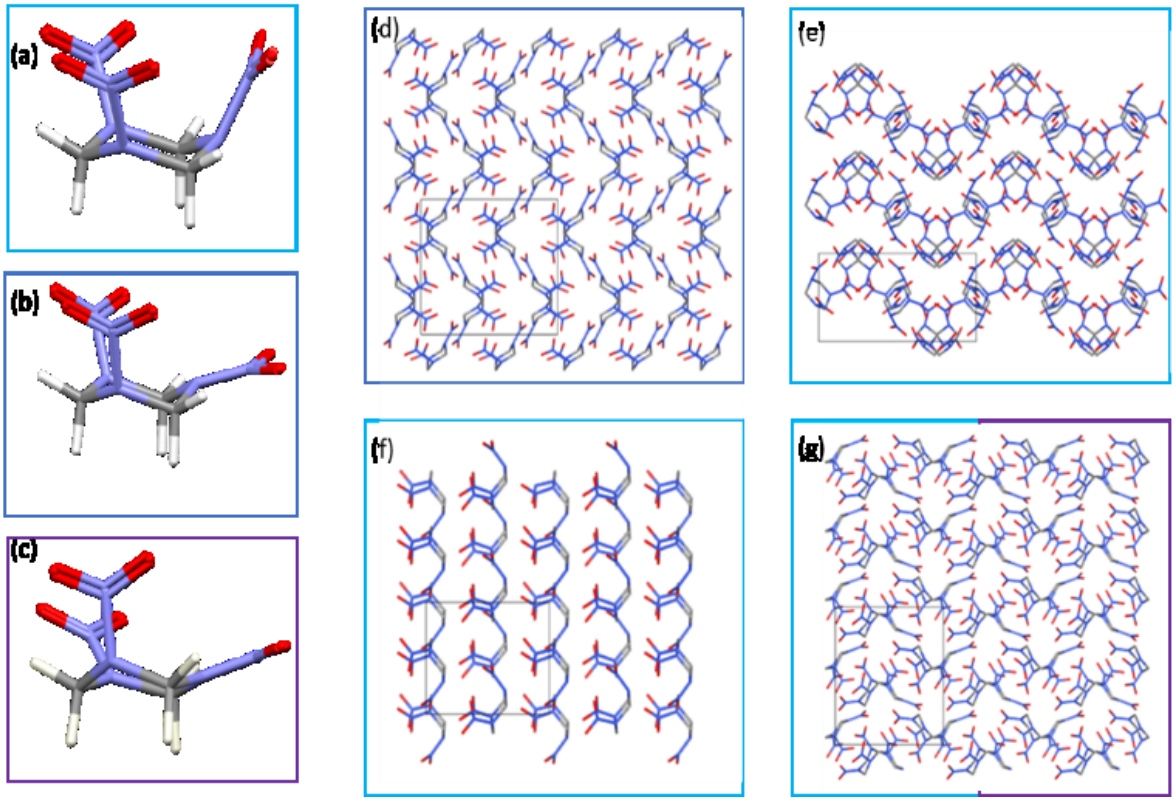

Fig. 1 Structures of RDX showing differences in (a-c) molecular conformations and (d-g) crystal packing arrangements. (a) AAA, (b) AAE, and (c) AAI conformations, denoting A- axial, E- equatorial and I- intermediate positions of the nitro groups. (d) α-, (e) β-, (f) ε- , and (g) γ-polymorphic forms.

The issues associated with IS measurements have prompted a response from the modelling community to generate reliable structure/predication models. This has included investigating correlations between IS and bond dissociation energies,[3] electron density topologies,[4-5] crystal void space and compressibility[6] and electronic band gaps.[7,8] However, all of these methods tend to offer a more qualitative rationale for impact sensitivity, and are generally

restricted to chemically similar energetic molecules. In contrast, vibrational up-pumping has emerged as a reliable tool capable of successfully ranking a broad range of EMs according to their experimental IS values.[8-18]

In essence, the up-pumping model describes the ease with which the vibrational modes of a crystalline material (represented by the phonon density of states, g(ω)) can channel the energy from a mechanical impact event through its low energy external lattice modes to reach the localised molecular vibrations. A general schematic of the vibrational up-pumping process is shown in Figure 2. The initial mechanical impact induces a compressive wave in the crystalline solid, depositing energy in the three acoustic (translational) motions of the crystal. From here the energy quickly equilibrates across the continuum (or 'bath') of external phonon modes, *q*, with an upper bound Ω_{max} that typically falls around 200 $\pm$ 50 cm^{-1}.[11] The vibrationally excited phonon bath modes subsequently combine and conduit (up-pump) excess energy into high frequency internal (localised) molecular vibrations, *Q*.

The up-pumping process defines permitted phonon-phonon scattering pathways, in accordance with a general vibrational Hamiltonian,

$$H = H_q + H_Q + H_{q.Q} \quad \text{Equation 1}$$

where low energy external lattice modes (H_q) and the higher energy internal molecular modes (H_Q) are treated as unique, separable entities. The third term of Equation 1 refers to the conversion of energy between external and internal modes, and can be expanded to first order by a Fermi golden rule formalism as

$$H_{q.Q} \propto \left|V^{(3)}\right| \delta(Q - q_1 - q_2) \quad \text{Equation 2}$$

where $V^{(3)}$ is the cubic anharmonic coupling constant that describes the strength of interaction between three vibrational modes and ensures energy conservation. While the values of $V^{(3)}$ are system specific, high resolution Raman spectroscopy and computational modelling work has found that the magnitude of $V^{(3)}$ is largely conserved for organic molecular EMs, including for HMX, RDX, TATB and PETN.[19-21] The explicit calculation of this anharmonic term is therefore omitted in this work. The remainder of Equation 2 is the two-phonon density of states, $\Omega^{(2)}$, which describes the scattering (combination) of two phonons (q_1, q_2) to create a third, higher energy phonon (Q). The permitted pathways include the scattering of two identical phonon bath modes (akin to the generation of an overtone state in vibrational spectroscopy), two non-identical phonon bath modes (akin to the creation of a combination mode vibrational state), or one phonon bath mode combining with a doorway vibrational mode, Q_D, that resides between 1-2 Ω_{max}. These Q_D modes are typically low-lying angle bend/torsional motions, often associated with e.g. C–NO_2 functional groups. The upper-limit accessible by two phonon scattering events is therefore 3Ω_{max}, and this defines the

upper boundary of the vibrational up-pumping window used in this work. The molecular vibrations contained within the window induce distortions of the weakest bonds in the energetic molecule. Thus, the up-pumping process localises the initial mechanical energy through the external vibrations into the local modes, resulting in activation of trigger linkages, leading to bond-breaking and initiation.[22-24] In our work we take the projection of $\Omega^{(2)}$ onto g(ω) over 1-3 Ω_{max} as a metric to describe how efficiently the crystal lattice of the EM can trap mechanical energy in its molecular vibrations.

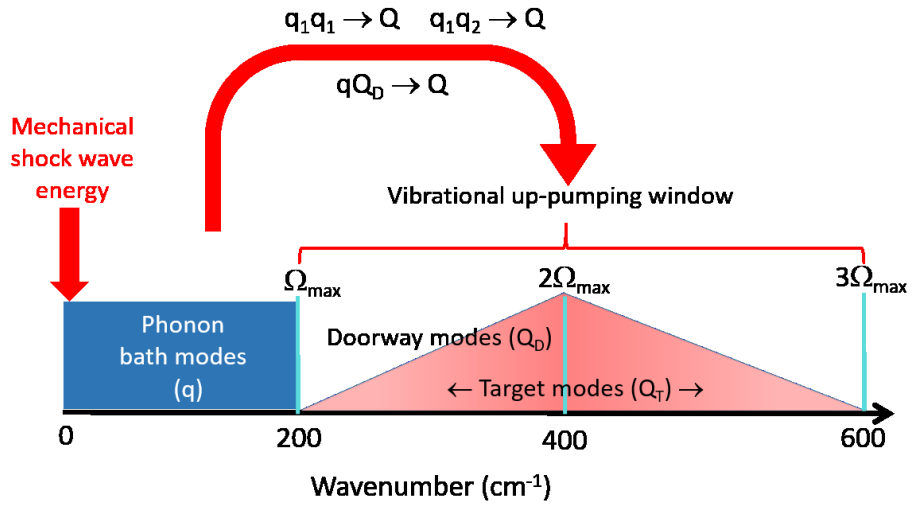

Fig 2: Schematic diagram of the vibrational up-pumping process.

With the up-pumping model having already demonstrated success for numerous well-known EMs,[8-18] we now turn our attention to RDX. This has been the subject of a number of previous reports. McNesby applied an up-pumping model using Raman spectroscopy data that successfully ranked the measured impact sensitivities of a number of EMs, including RDX.[14] Chauduri et al applied an up-pumping model to study the energy transfer at a hot-spot interface in RDX.[25] Chung et al demonstrated that lattice phonons dominate the thermal energy transfer to modes with significant nitrogen-nitrogen (NN) character in RDX,[26] and later quantified the three-phonon scattering rates and mode-to-mode scattering rates for energy transfer from phonons expressed across the Brillouin zone into the NN molecular vibrations.[27] Our own interests relate to the polymorphic nature of RDX, and in this regard this study was also motivated by our recent combined experimental and theoretical report that another well-known EM, FOX-7, was predicted to show a polymorphic dependency for IS.[28] Note in this work experimental validation proved impossible to obtain, as the act of measuring the IS for γ-FOX-7 induced a phase transition to α-FOX-7. Chaudhuri et al have also predicted using an overtone-based up-pumping model that IS varies for polymorphs of both CL-20 and HMX.[18]

Two crystalline phases (known as the α-[29] and β-forms[30]) of RDX have been structurally characterised at ambient conditions. A third polymorph, the ε-form,[31] can be produced under high-pressure (5.2 GPa) and high-temperature (450 K) conditions. This form can be recovered

under ambient pressure, low temperature conditions (< 230 K), where it has been structurally characterised. A fourth phase, the γ-phase, has been obtained by compressing a single crystal of α-RDX to 3.9 GPa at ambient temperature.[32] A fifth polymorph, the δ-phase, was identified in a high-pressure Raman spectroscopy study, but its crystal structure has not yet been determined.[33] Crystal-packing arrangements of the four structurally characterised polymorphs are shown in Figure 1.

As well as exhibiting different crystal-packing arrangements, the polymorphs of RDX also show different molecular conformations. While the triazine ring always maintains a chair conformation, the three pendant nitro groups vary in their orientations (see Figure 1). In α-RDX, all molecules have two nitro groups in the axial (A) position and one in the equatorial (E) position, to give the AAE conformation. For the β- and ε- forms, all molecules adopt the AAA conformation, whereas the asymmetric unit of γ-RDX contains one molecule in the AAA conformation, and a second in the AAI conformation. The AAI conformation can be regarded as intermediate between AAE and AAA.

In this paper we report on the application of the vibrational up-pumping model to predict the IS for four polymorphs of RDX. The model provides a convenient platform to discuss structure/property relationships, permitting the effects of molecular conformation, crystal packing, and hydrostatic compression on IS to be probed in some detail for this important EM. Finally, we show how the predicted IS values for the RDX polymorphs rank alongside other EMs previously reported by the vibrational up-pumping model.

Computational modelling

Input geometries for the four polymorphs of RDX were obtained from the Cambridge Structural database[34] (codes: CTMTNA11,[35] CTMTNA04,[30] CTMTNA07,[31] and CTMTNA02[32]) and subjected to full optimisation using CASTEP version 17.21 (PBE functional with dispersion correction TS for the α- and β-polymorphs and G06 for the ε- and γ-polymorphs, norm-conserving pseudopotentials coupled to a plane wave basis set expressed at 950 eV, Brillouin zone sampling of 0.05 $Å^{-1}$ and an FFT grid set to 2.0).[36-38] Input file preparation was aided using Seek-path.[39] Geometry optimisation convergence criteria were as follows: atomic forces < 5.0×10^{-3} eV/Å, change in energy per atom < 2.0×10^{-6} eV/atom, unit-cell stress < 5.0×10^{-3} GPa and maximum atomic displacement 5×10^{-4} Å. For the γ-form, an external pressure of 3.9 GPa was applied during optimisation. In addition, to elucidate whether any differences in the calculated phonon spectra for the high pressure phase could be attributed directly to the external pressure (i.e. mode hardening), optimisations were repeated for γ- and α-RDX in the absence/presence of a 3.9 GPa external pressure, respectively.

Following geometry optimisation (unit-cell parameters quoted in the ESI; the resulting deviations in unit cell volumes are of the order 4-7%, indicating that reliable optimised structures have been obtained),[40] phonon calculations were carried out at the Brillouin zone gamma-point only using density functional perturbation theory (DFTP).[41] The acoustic sum rule was applied analytically. All structures returned all positive vibrational frequencies with the exception of β-RDX, which initially showed five low-lying imaginary frequencies (at -18, -17.5, -15.6, -6.1 and -2.6 cm^{-1}). Tightening the fine FFT grid (from 2.0 to 4.0) reduced this to one (at -9 cm^{-1}). As this is an experimentally characterised polymorph it is likely that the imaginary frequency has arisen due to further numerical instabilities in the geometry optimisation process, rather than an indication of a metastable state. However, as the predicted IS metric increased by less than 3% upon removal of four of the five imaginary frequencies, it is unlikely that further pursuing the calculation quality, by further tightening of the convergence criteria, would result in any appreciable differences in the predicted impact sensitivity value.

All resulting g(ω) plots were presented with a Gaussian smearing width of 5 cm^{-1}. Assignment of Ω_{max} was made in each case by tracking the displacement of the centre of mass (CoM) for all molecules in a unit cell for each eigenvector, backed up with mode visualisation using Jmol.[42] When the CoM displacements fell below 10 % of the maximum value, the phonons were considered to be more localised in nature than delocalised, thus marking the transition from external lattice mode to molecular-based vibrations. These plots are available in the ESI. The shock temperature, T_{shock}, i.e. the superheated phonon quasi-temperature adopted to simulate the mechanical impact event, is obtained from the ratio of the bulk heat capacity to the phonon bath heat capacity, C_{tot}/C_{ph} (also shown in the ESI). Based on previous work a C_{tot}/C_{ph} ratio of 5.00 was set to 3278 K (calculated from the adiabatic compression of a model organic crystal).[16]

To successfully capture the IS of RDX, our up-pumping model has evolved to include an additional scattering pathway. Our previous model considered: (1) scattering of two external phonons into the doorway region (i.e. 1-2 Ω_{max}), followed by (2) scattering of an external phonon with a doorway mode into the region 2-3 Ω_{max}. Though successful for many systems, this model severely underestimated the predicted IS of RDX. We have resolved this issue by now allowing the scattering in pathway (2) to also up-pump density onto the doorway region, without sacrificing the predictive power across the previously reported EM data set. Further discussion is provided in the ESI.

Results and Discussion

The calculated g(ω) for all optimised structures is shown in Figure 3(a). The same computational approach has previously been shown to provide excellent agreement with the experimental inelastic neutron scattering (INS) spectrum of α-RDX.[43] From g(ω) we obtained

the phonon scattering (up-pumping) pathways, $\Omega^{(2)}$, also shown in Figure 3(a) using the parameters listed in Table 1. To ensure that this process generates up-pumping values that can be compared across different crystal structures, it is important that the data are normalised. In this work, g(ω) was normalized to the number of modes in the phonon bath prior to generating $\Omega^{(2)}$. This allows us to compare different phonon spectra on an absolute scale. In addition, the integral of the overlap between $\Omega^{(2)}$ and g(ω) within the up-pumping window is divided by the number of molecules in the unit cell. The latter normalization step is to account for the localisation of phonon energy after up-pumping. Further details are available in the ESI.

It is immediately apparent that the β- and ε-forms have very similar g(ω) (and hence $\Omega^{(2)}$), which arises due to the same molecular conformation (AAA) being present in their respective crystallographic unit cells. This also suggests that the intermolecular interactions contained in these two polymorphs are weak. This agrees with the lower lattice energy previously reported for β-RDX compared to α-RDX,[43] and the observation that ε-RDX readily transforms to α-RDX on heating above 230 K.[31] α-RDX has a notably different up-pumping window, which reflects the different molecular conformation (AAE) in this polymorphic form. Overall γ-RDX is the biggest outlier, with a significantly higher Ω_{max} and a more densely populated up-pumping window that contains molecular vibrations for two molecular conformations (AAA and AAI).

These differences in g(ω) and $\Omega^{(2)}$ are carried through to the predicted up-pumping intensities (Table 1). Our calculations suggest that the IS values for the β- and ε-forms are very similar, with α-RDX being higher, and γ-RDX being even higher. These predictions therefore suggest that the molecular conformation of RDX is critically important: maintaining the AAA conformation and varying the crystal packing observed for the β- and ε-polymorphs has little effect, while switching to the AAE conformation presents more vibrational states to boost and trap $\Omega^{(2)}$. The same observation holds for γ-RDX, where the two molecular conformations (AAA and AAI) display even more vibrational modes in the up-pumping window (Figure 3(a)).

The next question that arises from the up-pumping model is why the phonon bath for γ-RDX extends so high compared to the other three polymorphs. Animation of the vibrational modes leading up to Ω_{max} (*ca*. 100-164 cm^{-1} for α-, β- and ε–RDX; 100-268 cm^{-1} for γ-RDX) shows the expected amalgamated mode (*Y*) behaviour, where molecular deformation modes combine with the lattice motions (the six translational/rotational degrees of freedom, per molecule). For the ambient-pressure phases, these eigenvectors (six per molecule) involve various combinations of -NO_2 twisting motions, while the first clusters of vibrational modes that fall within the up-pumping windows describe various combinations of N-NO_2 out-of-plane motions. For the high-pressure γ-phase, both of these molecular motions are contained in the phonon bath, resulting in a greater number of amalgamated modes (eight per molecule) for γ-RDX compared to the ambient-pressure phases (Table 1). Moreover, the

extent of lattice mode behaviour is significantly more pronounced for γ-RDX, as demonstrated by tracking the changes in the CoM for each of the eigenvectors (see ESI).

Table 1: Parameters used to calculate $\Omega^{(2)}$ for polymorphs of RDX. Ω_{max} denotes the top of the phonon bath, *Z* the number of molecules in each unit cell, *Y* the number of amalgamated vibrations per molecule in the phonon bath regions, and T_{shock} is the temperature adopted for the phonon bath modes. The up-pumped density is the projection of $\Omega^{(2)}$ onto g(ω) per molecule in the up-pumping window 1-3 Ω_{max}.

POLYMORPH	Ω_{MAX}	*Z*	*Z(6+Y)*	*Y*	T_{SHOCK} / K	UP-PUMPED DENSITY/Z / $\times 10^3$ A.U.
α-RDX	164	8	96	6	3265	48.1
β-RDX	164	8	96	6	3390	26.7
ε-RDX	164	4	48	6	3395	15.9
γ-RDX*	268	8	112	8	2820	176.2
α-RDX*	257	8	112	8	2835	67.0

*Optimised with 3.9 GPa external pressure

Thus, the question now becomes: why do the lattice and molecular vibrations separate less readily for γ-RDX? The most likely explanation is because this polymorph was subjected to external pressure during geometry optimisation. It has been noted that pressures of up to 4 GPa can be expected to produce a blue-shift in molecular-based vibrational frequencies on the order of 5-20 cm^{-1},[43] which is confirmed in the observed changes in mode distributions for the polymorphs of RDX noted above. It is also well known that external phonon frequencies tend to harden substantially with pressure, as noted by the Debye temperature dependence on pressure.[44] In an attempt to quantify directly the effect of the external pressure on predicted IS values within the up-pumping model, geometry optimisation for γ-RDX was repeated in the absence of the external pressure. Unfortunately, this caused the unit cell to expand by over 30%, resulting in an unrealistic representation of the high-pressure phase. As an alternative, α-RDX was re-optimised under 3.9 GPa external pressure conditions to observe how this changes g(ω), $\Omega^{(2)}$, and the predicted up-pumped density (Figure 3(b)). The unit-cell volume of compressed α-RDX decreased to levels comparable with γ-RDX (see ESI). On analysis of the resulting g(ω), a considerable increase in the value of Ω_{max} is immediately apparent, placing Ω_{max} at 257 cm^{-1}, in close alignment with γ-RDX (Table 1). The amalgamated mode count for compressed α-RDX also matches that for γ-RDX (Table 1), while the remaining external modes of vibration have experienced mode hardening of *ca*. 5-10 cm^{-1}. The corresponding predicted up-pumping metric derived from the projection of $\Omega^{(2)}$ onto g(ω) shown in Figure 3(b) has increased compared to the non-compressed form (Table 1).

Thus, the effect of applying an external pressure to α-RDX is significant, and by extension will likely also play a similar role on the high pressure γ-form.

While the external pressure undoubtedly plays a role in boosting the predicted IS for γ-RDX, other factors must be at work to account for the near three-fold difference still observed between compressed α-RDX and γ-RDX. To account for this we now turn to the doorway region, which is the first half of the up-pumping window (i.e. 1-2 Ω_{max}). This is a particularly important region because in the up-pumping model the doorway modes both contribute to and capture the up-pumped energy. Given that the γ-form contains two molecular conformations, partial g(ω) plots were constructed to show the contribution from both conformations (see Figure 3(c)). Crucially this analysis shows that peaks at 330-360 cm^{-1}, which are attributed to the AAI conformation alone, help to populate the doorway region. These eigenvectors are best characterised (visually) as N–NO_2 bond stretching and ring deformation modes. The analogous vibrations for the AAA conformation fall at 360-390 cm^{-1}, where they occur alongside other AAI ring deformation modes. Similar eigenvectors are observed for the AAA conformer at 350-360 cm^{-1} in β-RDX and at 360-370 cm^{-1} in ε-RDX, while those associated with the AAE conformer in α-RDX appear at 340-350 cm^{-1}. Thus, these modes fall outside the doorway regions for all phases except for the γ-form.

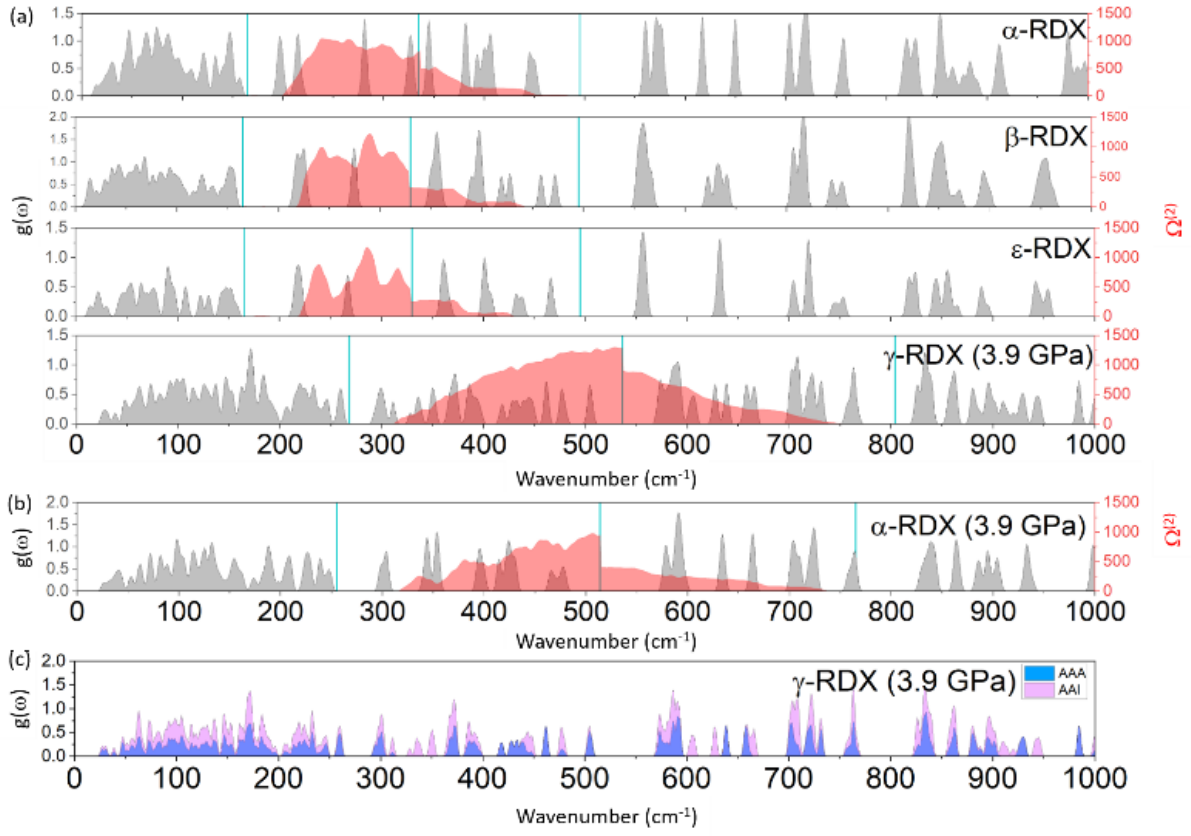

Fig. 3: Simulated vibrational spectra for RDX polymorphs. (a) g(ω) (grey) of the RDX polymorphs with $\Omega^{(2)}$ overlayed (red), vertical blue lines represent sequential multiples of Ω_{max}, with the up-pumping window defined by the 1-3 Ω_{max} limits. (b) Analogous data for α-RDX compressed at 3.9 GPa. (c) Partial g(ω) showing the contributions to the vibrational modes from conformers AAA and AAI in γ-RDX.

It is therefore apparent that two factors are responsible for the prediction of increased IS for the γ-form of RDX: (i) direct compression, which leads to shorter and stronger intermolecular interactions that influence the structure of the g(ω) bath region, and (ii) changes in molecular conformation that alter the distribution of molecular vibrations that fall in the up-pumping window.

As the predicted IS values for the different polymorphs of RDX are relative values, it is possible to rank them alongside those of other EMs that have been investigated using the same up-pumping model (see ESI). This is presented in Figure 4, from which a clear relationship is drawn – the more sensitive a material is to impact (i.e. the lower the mechanical stimulus needed to initiate the EM), the higher the calculated up-pumped density. Taking an experimental IS value for RDX of 13 J,[2] and assuming this corresponds to α-RDX, our prediction sits close to the curve. Note that, as experimental values are not known for the other polymorphs, we have plotted all corresponding data points at the same value on the x-axis. For completeness we also include the predicted variability for the FOX-7 polymorphs according to our up-dated up-pumping model (see ESI); this represents an update from our earlier publications.[16,28]

The differences in predicted impact sensitivities shown in Figure 4 are quite stark. β-RDX sits below α-RDX, but arguably still close to the curve, despite the presence of one imaginary frequency in its g(ω) which likely means its predicted IS is slightly underestimated. ε-RDX sits lower still, with a predicted sensitivity closer to α-FOX-7. γ-RDX sits well above it, approaching a value close to that of the highly sensitive ε-CL-20. This raises important questions considering the handling of RDX under shock-wave conditions. At 3-5.5 GPa shock loading, Patterson *et al.* reported *in situ* Raman spectra that corresponded to the α → γ phase transition.[45] Similarly, molecular dynamics simulations have also demonstrated that the α → γ transformation can occur readily under shock loading.[46] Our simulations therefore raise the intriguing possibility that if the α → γ phase transition could be suppressed, then the shock-sensitivity of RDX could be improved. In principle, this might be achieved by doping α-RDX with an additive that increases the α → γ transition pressure, thereby suppressing formation of the more sensitive γ-form. There are precedents that pressure-induced polymorphism can be tuned through crystal engineering strategies. For example, doping the well-known EM ammonium nitrate with a group 1 nitrate suppresses an undesirable temperature-induced phase transition that is responsible for the deterioration of its mechanical properties.[47] Doping has permitted high pressure polymorphs to be stabilized at ambient conditions,[48] and phase transitions have been pushed to higher pressures.[49]

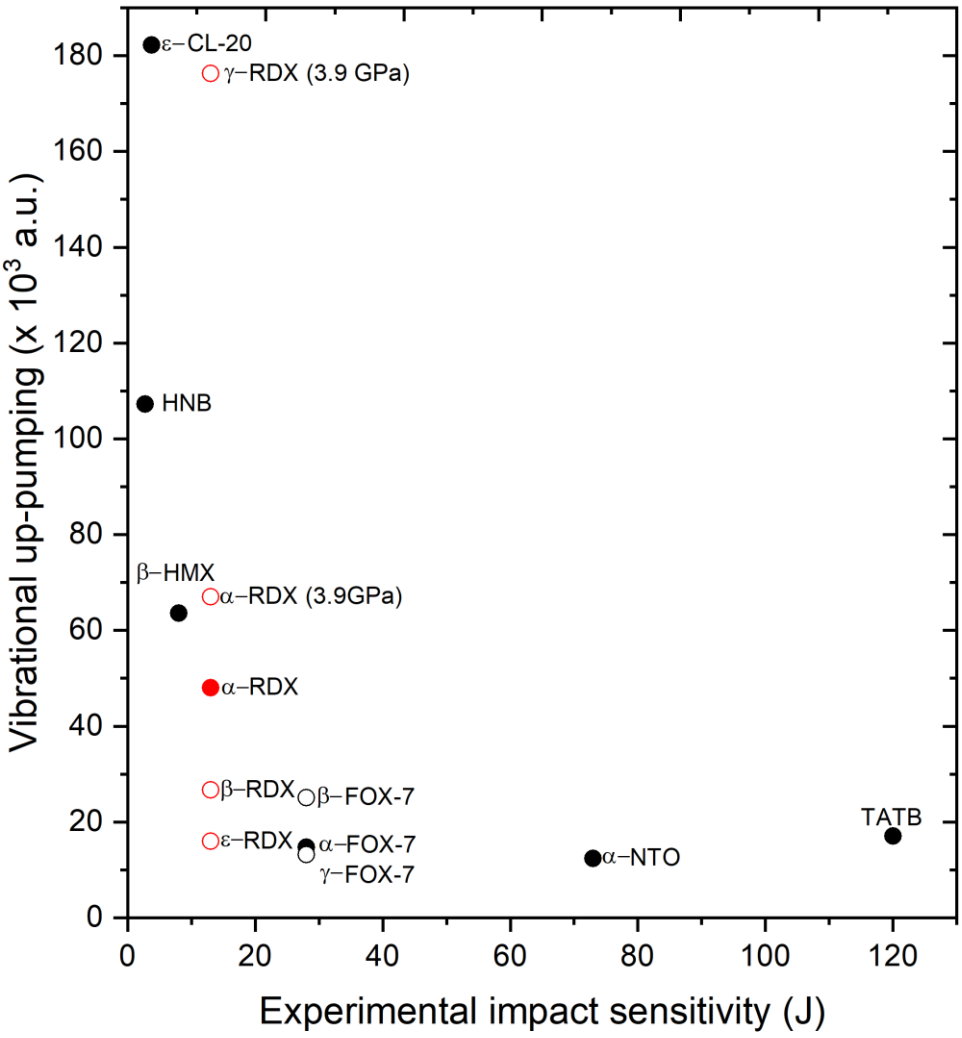

Fig. 4. Experimental IS values versus vibrational up-pumped densities for a range of EMs (see ESI), alongside predictions for the polymorphs of RDX, shown in red. Filled symbols correspond to experimentally measured data points, unfilled to predicted values only.

Conclusions

Through application of the vibrational up-pumping model, this work predicts that the impact sensitivity of RDX should show a strong polymorphic dependency. The high-pressure γ-form, which is accessible under shock-loading conditions, is predicted to be more prone to mechanochemical initiation. This is due to mode hardening through the presence of an external pressure, and to the presence of two molecular conformations in the crystallographic unit cell, AAA and AAI, which boosts the number of molecular vibrations in the up-pumping window to both contribute to and trap the two phonon density of states energy, $\Omega^{(2)}$. This suggests that if the α → γ phase transition could be suppressed, the shock sensitivity of RDX

could be reduced, thereby enhancing safety under operational conditions. The β- and ε-forms, which both comprise the AAA molecular conformation of RDX, are predicted to be less efficient at trapping $\Omega^{(2)}$ compared to the AAE conformation present in a-RDX. Consequently, vibrational up-pumping predicts that β- and ε-RDX should be less prone to mechanochemical initiation than α-RDX. This work further highlights the power of the vibrational up-pumping method to give new insights into important performance and safety metrics for energetic materials.

Supplementary material

See the supplementary material for further information on the vibrational up-pumping model, geometry optimisation and phonon processing data.

Acknowledgements

We thank Dr. Ranko Vrcelj (Centre for Defence Chemistry, Cranfield University, Defence Academy of the United Kingdom) and Dr. Malcolm J. Burns (Los Alamos National Laboratory) for helpful discussions. This material is based upon work supported by the Air Force Office of Scientific Research under award number FA8655-20-1-7000. We are grateful for computational support from the United Kingdom Materials and Molecular Modelling Hub, which is partly funded by EPSRC (EP/PO20194 and EP/TO22213), for which access was obtained via the UKCP consortium and funded by EPSRC grant ref EP/PO22561/1. ILC thanks the University of Edinburgh, School of Chemistry for the award of a PhD scholarship.

References

1. P. A. Davies*, J. Hazard. Mater*. **38**, 75 (1994).
2. R. M. Doherty and D. S. Watt, *Propellants, Explosives, Pyrotechnics*, **33**, 4 (2008).
3. B. M. Rice , S. Sahu and F. J. Owens , *J. Mol. Struct.: THEOCHEM*, **583**, 69 —72 (2002).
4. J. S. Murray , M. C. Concha and P. Politzer, *Mol. Phys.*, **107** , 89 —97, (2009).
5. A. A. Aina, A. J. Misquitta, M. J. S. Phipps and S. L. Price, **4**, 8614— 8625 (2019).
6. P. Politzer and J. S. Murray , Impact Sensitivity and Crystal Lattice Compressibility/Free Space, *J. Mol. Model.*, 2014, **20** , 2233.
7. H. Zhang , F. Cheung , F. Zhao and X. Cheng , Band Gaps and the Possible Effect on Impact Sensitivity for Some Nitro Aromatic Explosive Materials, *Int. J. Quantum Chem.*, 2009, **109** , 1547 —1552.
8. A. A. L. Michalchuk, M. Trestman, S. Rudić, P. Portius, P. T. Fincham, C. R. Pulham and C. A. Morrison, *J. Mat. Chem. A*, **7**, 19539–19553 (2019).
9. C. S. Coffey and E. T. Totton, *J. Chem. Phys.*, **76** , 949 —954 (1982).
10. F. J. Zerilli and E. T. Totton, *Phys. Rev. B*, **29** , 5891 —5902 (1984).
11. H. Kim and D. D. Dlott , *J. Chem. Phys.*, **93** , 1695 —1709 (1990).
12. A. Tokmakoff , M. D. Fayer and D. D. Dlott , *J. Phys. Chem.*, **97** , 1901 —1913 (1993).
13. D. D. Dlott and M. D. Fayer, *J. Chem. Phys.*, **92** , 3798—3812 (1990).
14. K. L. McNesby and C.S. Coffey, J. Phys. Chem. B, 101 3097-3194 (1997).
15. J. Bernstein, *J. Chem. Phys*. **148**, 084502 (2018).

16. A. A. L. Michalchuk, J. Hemingway and C. A. Morrison, *J. Chem. Phys.*, **154**, 064105 (2021).
17. S. V. Bondarchuk, *FirePhysChe*m, **2**, 334-339 (2022).
18. X. Bidault and S. Chaudhuri, *RSC. Adv*., **12**, 31282-31292 (2022).
19. S. D. McGrane and A. P. Shreve, *J. Chem. Phys.*, **119**, 5834–5841 (2003).
20. S. D. McGrane, J. Barber and J. Quenneville, *J. Phys. Chem. A* **109**, 9919–9927 (2005).
21. Ye and M. Koshi, *J. Phys. Chem. B* **110**, 18515–18520 (2006).
22. N. C. Cole-Filipiak, R. Knepper, M. Wood and K. Ramasesha, *J. Phys. Chem. A*. **125**, 7788-7802 (2021).
23. G. Yu, Y. Zeng, W. Guo, H. Wu, G. Zhu, Z. Zheng, X. Zheng, Y. Song and Y. Yang, *J. Phys. Chem. A* **121**, 2565-2571 (2017).
24. A. A. L. Michalchuk, S. Rudić, C. R. Pulham and C. A. Morrison, *Phys. Chem. Chem. Phys.*, **20**, 29061–29069 (2018).
25. K. Joshi, M. Losada and S. Chaudhuri, *J. Phys. Chem. A*. **120**, 477-489 (2016).
26. B. Kraczek and P.W. Chung, *J. Chem. Phys*. **138**, 074505 (2013).
27. G. Kumar, F. G. VanGessel, L. Munday and P. W. Chung, *J. Phys. Chem. A*. **125**, 7723-7734 (2021).
28. A. A. L. Michalchuk, S. Rudić, C. R. Pulham and C. A. Morrison, *Chem. Commun.*, **57**, 11213–11216 (2021).
29. P. Hakey, W. Ouellette, J. Zubieta and T. Korter, *Acta Crystallographica Section E: Structure Reports Online*, **64**, o1428–o1428 (2008).
30. D. I. A. Millar, I. D. H. Oswald, D. J. Francis, W. G. Marshall, C. R. Pulham and A. S. Cumming, *Chem. Commun.*, 562–564 (2009).
31. D. I. A. Millar, I. D. H. Oswald, C. Barry, D. J. Francis, W. G. Marshall, C. R. Pulham and A. S. Cumming, *Chem. Commun.*, **46**, 5662–5664 (2010).
32. A. J. Davidson, I. D. H. Oswald, D. J. Francis, A. R. Lennie, W. G. Marshall, D. I. A. Millar, C. R. Pulham, J. E. Warren and A. S. Cumming, *CrystEngComm*, **10**, 162–165 (2008).
33. J. A. Ciezak, T. A. Jenkins, Z. Liu and R. J. Hemley, *J. Phys. Chem. A*, **111**, 59–63 (2006).
34. C. R. Groom, I. J. Bruno, M. P. Lightfoot and S. C. Ward, *Acta Crystallogr. Sect. B Struct. Sci. Cryst. Eng. Mater.*, **72**, 171–179 (2016).
35. V. V. Zhurov, E. A. Zhurova, A. I. Stash, A. A. Pinkerton CCDC 1432690: Experimental Crystal Structure Determination (2015), DOI: 10.5517/cc1k2tt8
36. S. J. Clark, M. D. Segall, C. J. Pickard, P. J. Hasnip, M. J. Probert, K. Refson and M. C. Payne, *Zeitschrift fuer Krist.*, **220**, 567–570 (2005).
37. A. Tkatchenko and M. Scheffler, *Phys. Rev. Lett.*, **102**, 073005 (2009).
38. S. Grimme, *J. Comput. Chem*., **27**, 1787 (2006).
39. Y. Hinuma, G. Pizzi, Y. Kumagai, F. Oba, and I. Tanaka, *Comp. Mat. Sci.* **128**, 140-184 (2017). DOI: 10.1016/j.commatsci.2016.10.015
40. J. Binns, M. R. Healy, S. Parsons and C. A. Morrison, *Acta Crystallogr. Sect. B Struct. Sci. Cryst. Eng. Mater.*, **70**, 259–267 (2014).
41. K. Refson, P. R. Tulip and S. J. Clark, *Phys. Rev. B - Condens. Matter Mater. Phys.*, **73**, 155114 (2006).
42. Jmol: an open-source Java viewer for chemical structures in 3D., http://www.jmol.org/.
43. S. Hunter, T. Sutinen, S. F. Parker, C. A. Morrison, D. M. Williamson, S. Thompson, P. J. Gould and C. R. Pulham, J*. Phys. Chem. C.* **117**, 8062-8071 (2013).
44. S. K. Sharma, *Solid State Communications*, **149**, 2207-2209 (2009).
45. J. E. Patterson, Z. A. Dreger and Y. M. Gupta, *J. Phys. Chem. B*., **111**, 10897-10904 (2007).

46. D. C. Sorescu and B. M. Rice, *J. Phys. Chem. C*., 2016, **120**, 19547-19557 (2016).
47. C. Oommen and S. R. Jain, *J. Hazard. Mater*., **67**, 253-281 (1999).
48. F. Safari and A. Katrusiak, *J. Phys. Chem. C*., **125**, 23501-23509 (2021).
49. W.-P. Hsieh and Y.-H. Chien, *Scientific Reports*, **5**, 8532 (2015).

Is the impact sensitivity of RDX polymorph dependent?

Imogen L. Christopher,[1] Colin R. Pulham,[1] Adam A. L. Michalchuk,[2,*] and Carole A. Morrison[1,*]

[1]School of Chemistry and EaSTCHEM Research School, University of Edinburgh, David Brewster Road, The King's Buildings, Edinburgh, EH9 3FJ, UK

[2]School of Chemistry, University of Birmingham, Edgbaston, Birmingham, B15 2TT, UK.

Supplementary Information

Vibrational up-pumping model

To allow direct comparison of the vibrational up-pumping results alongside other energetic materials (EMs), the phonon DoS was normalised according to the number of modes in the phonon bath: *Z*(6+*Y)*, where *Z* is the number of molecules in the unit cell and *Y* is the number of amalgamated modes (per molecule) in the phonon bath. The resulting DoS was then up-pumped via a number of scattering routes, which combine two lower frequency modes (ω_1, ω_2) to transfer phonon population to a higher frequency mode (ω_3), ensuring energy conservation during the scattering processes, according to the following:

1. External lattice phonon self-scattering (i.e. $\omega_1 + \omega_1 \rightarrow \omega_3$), where $\omega_3 = \frac{\omega_1}{2}$. This is akin to overtone mode generation and excites vibrational bands in the region $\Omega_{max} - 2\Omega_{max}$. The phonon population transferred in this process is taken as $\frac{g(\omega_1, T_{shock})}{2} - g(\omega_3, T = 300\ K)$
2. External lattice phonon (ω_1) scattering with a doorway mode (ω_2) to excite a band between $\Omega_{max} - 2\Omega_{max}$ with population transfer according to $g(\omega_1, T_{shock}) + g(\omega_2, T = 300\ K) - g(\omega_3, T = 300\ K)$.
3. External lattice phonon (ω_1) scattering with an excited doorway mode (ω_2) to excite a band between $2\Omega_{max} - 3\Omega_{max}$, with population transfer according to $g(\omega_1, T = 300K) + g_{excited}(\omega_2) - g(\omega_3, T = 300\ K)$. This process represents the second up-pumping stage in our previously reported two-step up-pumping model.

The up-pumped multi-phonon density of states $\Omega^{(2)}$ are subsequently projected onto the fundamental vibrational bands to identify how much of the up-pumped energy is 'captured' by the material. Finally, the resulting projected multi-phonon density of states is normalized with respect to the number of molecules *Z* contained in the unit cell, accounting for the localization of energy into individual molecules at this stage.

We note that the normalisation scheme adopted for the DoS, $\Omega^{(2)}$ and the resulting $\Omega^{(2)}$/DoS overlap can follow a number of routes. We pursued a number of options in this work, and noted that while small fluctuations in the vibrational up-pumping metric were obtained, overall the trend in relative values across the set of EMs explored in this work varied by only small amounts. Small alterations did arise for the relative predicted sensitivities of β-FOX-7 with respect to the α- and γ-forms, however, with the ranking now listed as $\beta > \alpha > \gamma$ in the main text, compared to $\alpha > \beta > \gamma$ in our previous report.[1] Experimental measurement of the impact sensitivities for the β- and γ- polymorphs of FOX-7 remain elusive, as β-FOX-7 only exists at high temperatures and is not recoverable under ambient conditions, and our earlier report demonstrated that γ-FOX-7 converts to α-FOX-7 during mechanical impact sensitivity testing.[1] The critical observation, that $\alpha > \gamma$, is maintained in our new normalisation scheme. This outcome therefore continues to suggest that layered molecular crystal packing arrangements appear to reduce the sensitivity of energetic materials to mechanical initiation, by reducing their ability to up-pumping vibrational energy.

This up-pumping and normalisation scheme represents an update from our earlier reports.[1,2]

Table S1: Parameters used to calculate $\Omega^{(2)}$ for the other EMs reported in the main text. *Z* denotes the number of molecules in each unit cell, *Y* is the number of amalgamated vibrations per molecule in the phonon bath regions, and T_{shock} is the temperature adopted for the phonon bath modes. The up-pumped density is the projection of $\Omega^{(2)}$ onto g(ω), per molecule, in the up-pumping window 1-3 Ω_{max}.

Structure	Ω_{max}/cm^{-1}	*No. ext. modes* ($< \Omega_{max}$)	*Z*	*Y*	T_{shock}/K	*Up-pumped density/Z* / $\times 10^3$ *a.u.*	*Exp IS /J*	*Ref.*
HNB	155	30	2	18	3423	107.3	2.75	3
ε-CL20	222	88	4	64	3278	182.2	3.75	4
β-HMX	200	34	2	22	3488	63.5	8	4,5
α-FOX7	180	36	4	12	3278	14.7	28	6,7
β-FOX7	162.5	36	4	12	3278	25.1	Not known	-
γ-FOX7	158	72	8	24	3121	13.2	Not known	-
α-NTO	216	64	8	16	2643	12.4	72.75	5
TATB	151	24	2	12	4399	17.1	120	5

Geometry optimisation results

Table S2: Experimental and optimised unit cell parameters for the polymorphs of RDX

POLYMORPH	A / Å	B / Å	C / Å	$\alpha = \beta = \gamma$ / °	V / Å^3	ΔV %
α-RDX (EXP)	11.4425(3)	10.6106(3)	13.1558(4)	90	1597.27	
α-RDX (CALC)	11.6124	10.8685	13.5028	90	1704.19	+6.69
α-RDX (CALC)*	10.9414	10.1205	12.9049	90	1429.01	–
β-RDX (EXP)	15.1267(11)	7.4563(6)	14.3719(11)	90	1620.99	
β-RDX (CALC)	15.4375	7.6571	14.5923	90	1724.89	+6.41
ε-RDX(EXP)	7.519(4)	11.643(5)	9.176(4)	90	803.4	
ε-RDX (CALC)	7.6827	12.044	9.0929	90	841.40	+4.52
γ-RDX (EXP)	12.5650(19)	9.4769(6)	10.9297(9)	90	1301.48	
γ-RDX (CALC)*	12.8616	9.5927	11.1448	90	1375.02	+5.65

*Optimised with 3.9 GPa external pressure. This is the experimentally determined pressure for the $\alpha \rightarrow \gamma$ phase transition.

Phonon processing data

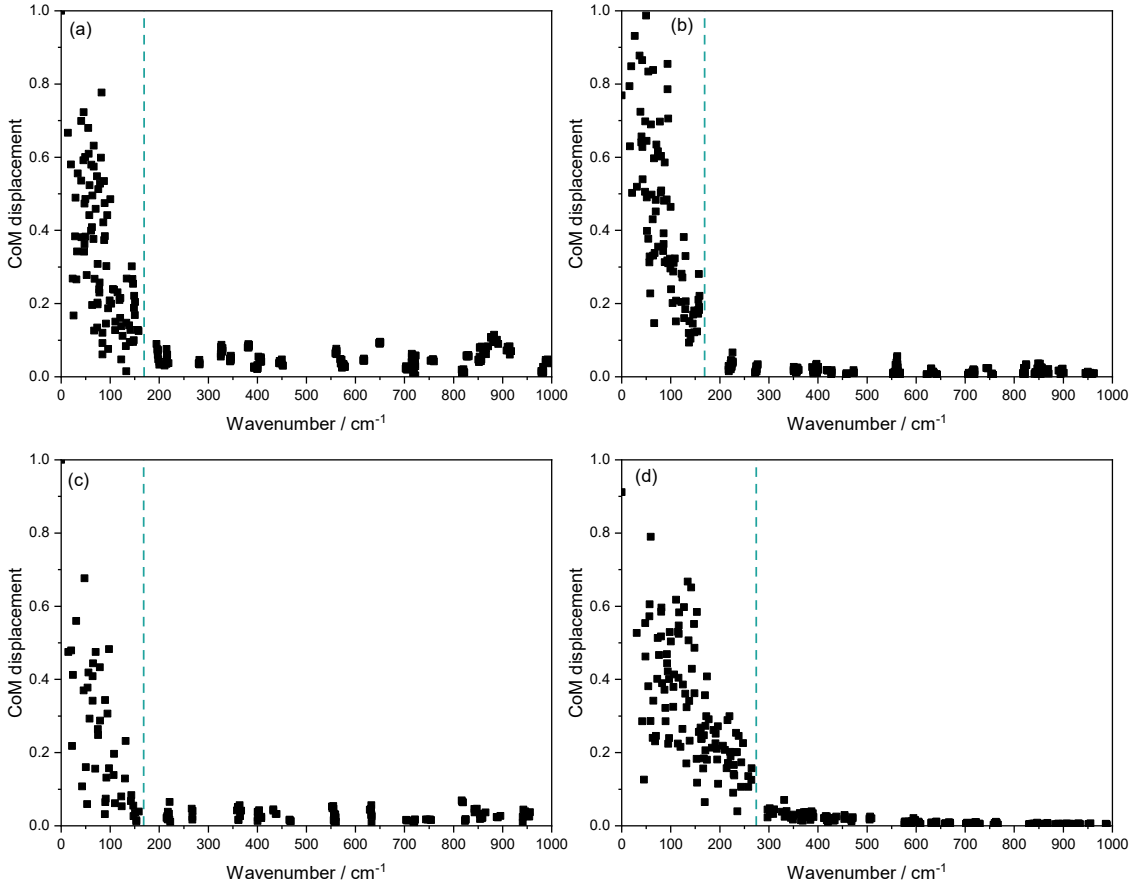

Figure S1: Centre of mass (CoM) displacements vs. wavenumber plots for (a) α- (b) β- (c) ε- and (d) γ-forms of RDX. Blue dotted lines mark the positions of Ω_{max}.

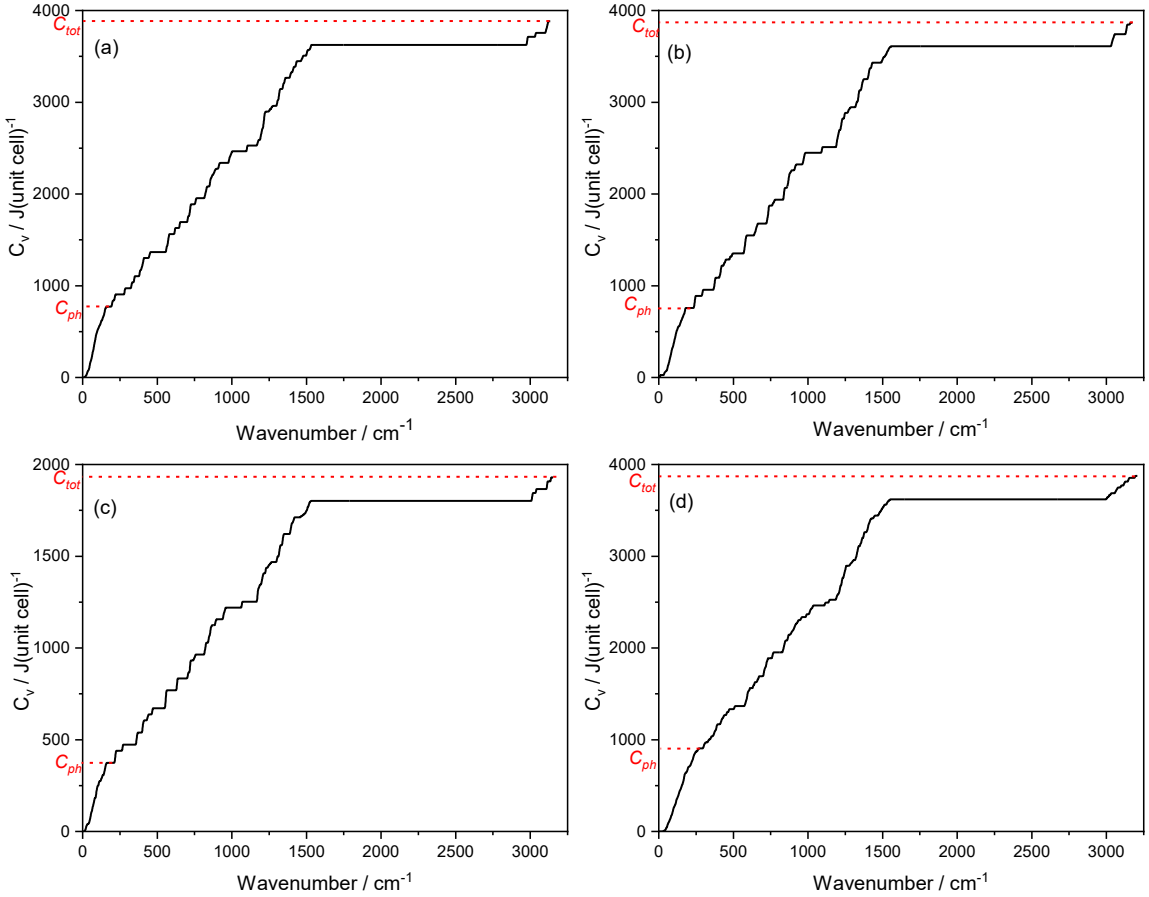

Figure S2: Cumulative heat capacities of the RDX polymorphs (a) α- (b) β- (c) ε- and (d) γ-forms. Values of C_{tot} and C_{ph} *(i.e. phonon)* are marked by red dotted lines, resulting in C_{tot}/C_{ph} ratios of 4.98, 5.17, 5.18 and 4.30 for (a)-(d), respectively. Based on a ratio of C_{tot}/C_{ph} of 5.00 equating to T_{shock} = 3278K from earlier work,[2] this yields T_{shock} values of 3264, 3389, 3396 and 2819 K for (a) – (d), respectively.

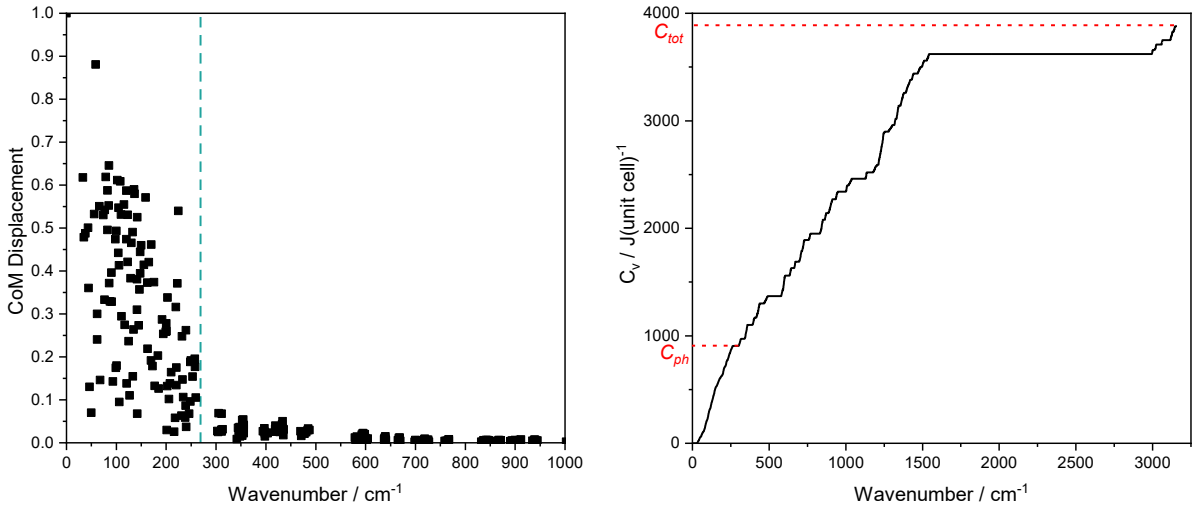

Figure S3: (a) CoM displacement (Ω_{max} marked by vertical dashed line) and (b) cumulative heat capacities for α-RDX, re-optimised at 3.9 GPa, yielding a C_{tot}/C_{ph} ratio of 4.32 and a T_{shock} value of 2835 K

References

1. A. A. L. Michalchuk, S. Rudić, C. R. Pulham and C. A. Morrison, *Chem. Commun.*, 2021, **57**, 11213–11216.
2. A. A. L. Michalchuk, J. Hemingway and C. A. Morrison, Predicting the impact sensitivities of energetic materials through zone-center phonon up-pumping, *J. Chem. Phys.*, 2021, **154**, 1–11.
3. W. S. Wilson, D. E. Bliss, S. L. Christian, and D. J. Knight, *Explosive Properties of polynitroaromatics* (Defence Technical Information Centre, Fort Belvoir, VA, 1990).
4. R. L. Simpson, P. A. Urtiew, D. L. Ornellas, G. L. Moody, K. J. Scribner, and D. M. Hoffman, Propellants, Explos., Pyrotech. **22**, 249 (1997).
5. C. B. Storm, J. R. Stine, and J. F. Kramer, in *Chemistry and Physics of Energetic Materials*, edited by S. N. Bulusu (Springer Netherlands, Dordrecht, 1990), pp. 605–639.
6. B. M. Rice and J. J. Hare, J. Phys. Chem. A **106**, 1770 (2002).
7. I. J. Lochert, *FOX-7—A New Insensitive Explosive* (DSTO Aeronautical and Maritime Research Laboratory, Victoria, Australia, 2001).